

RUILAI LIU (ORCID: 0000-0001-6320-9889)^{1,2}, JIAPENG HU (ORCID: 0000-0003-4382-1418)¹
JUIYE RAU (ORCID: 0000-0002-7838-6818)¹, HAO LIN (ORCID: 0000-0003-1587-9444)¹
HUAN HE (ORCID: 0000-0003-3460-2491)¹, BIAO GAO (ORCID: 0000-0002-8447-7724)³
WENLIANG LAI (ORCID: 0000-0001-7162-4716)⁴

SYNTHESIS AND CHARACTERIZATION OF TiO₂/ZSM-5 PHOTOCATALYSTS FOR DEGRADATION OF RHODAMINE

ZSM-5 synthesized by the hydrothermal method from raw kaolin clay was used as support to prepare TiO₂/ZSM-5 catalysts via the sol-gel method. All prepared samples were characterized by X-ray fluorescence spectrometry (XRF), X-ray diffraction (XRD), scanning electron microscopy (SEM), Fourier transform infrared (FT-IR), ultraviolet-visible spectroscopy (UV-Vis), transmission electron microscopy (TEM), particle size analysis and surface area measurement. The photocatalytic performance of TiO₂/ZSM-5 was investigated based on rhodamine B (RhB) removal under UV radiation (450–600 nm). The results showed that the kaolin clay was successfully transformed into ZSM-5. The BET surface area and pore size distribution of the synthesized ZSM-5 were 364 m²/g and 0.54 nm, respectively. SEM and TEM revealed that TiO₂ nanoparticles were well distributed on the surface of ZSM-5. The composite TiO₂/ZSM-5 catalyst showed 98.53% removal, which is higher than that of pure TiO₂ (80.13%) due to adsorption and degradation of RhB (5.0 mg/dm³) under 60 min UV light irradiation at 1 g/dm³ photocatalyst loading. The synergistic effect of TiO₂ and ZSM-5, including adsorption, conduction band electron (e⁻), and valence-band holes (h⁺), makes the composite superior to pure TiO₂, showing its potential for the degradation of organic dye.

¹College of Ecological and Resource Engineering, Fujian Provincial Key Laboratory of Eco-Industrial Green Technology, Wuyi University, Wuyishan 354300, China.

²College of Materials and Environmental Engineering, Fujian Polytechnic Normal University, Fuqing 350300, Fujian, China.

³School of Tourism and Geography Science, Baicheng Normal University, Baicheng, Jilin 137000, China.

⁴Graduate School of Environmental Management, Tajen University, Pingtung, Taiwan, corresponding author, email address: lai@tajen.edu.tw

1. INTRODUCTION

In the past few years, the life expectancy of people has greatly improved owing to the development of science and technology, however, significant environmental pollution has been simultaneously generated by artificial activities. To reduce environmental pollution, many researchers have paid great attention to semiconductor photocatalytic techniques for cleaning trace pollutants in air and water [1, 2]. To date, different semiconductor photocatalysts have been reported, including ZnO [1], Ag_3PO_4 [3], SnO_2 [4], WO_3 [5], Bi_2O_3 [6] and TiO_2 [7]. TiO_2 is an n-type semiconductor with a bandgap of 3.6 eV [7]. It has been widely used as a photocatalyst for environmental remediation of pollutants owing to its biological and chemical inertness, strong oxidizing power, nontoxicity, and long-term stability against photo and chemical corrosion. After irradiation of TiO_2 with UV light, electron and hole pairs can be produced, which effectively decompose organic pollutants into CO_2 and H_2O [8].

Recently, many researchers have focused on the production of TiO_2 nanoparticles, but their aggregation in suspension limits their applications in photocatalytic systems. Furthermore, the photocatalytic activity of TiO_2 is greatly influenced by the surface area, particle size, and porosity [9]. Enhancing the surface area of TiO_2 is the most effective way of improving the efficiency in photocatalytic oxidation reactions [9]. Many researchers immobilized TiO_2 nanoparticles on solid support materials to overcome these drawbacks resulting from synergistic effects. Activated carbon, Al_2O_3 , and zeolites are promising materials to support TiO_2 [10]. Among other support materials, zeolites are widely used owing to their several advantages such as low cost, high specific surface area, hydrophobicity/hydrophilicity, tunable properties, and eco-friendliness nature [11].

Zeolite Socony Mobil-5 (ZSM-5) has been widely used in many important catalytic reactions owing to its special pore structure [11]. ZSM-5 is also very popular as a semiconductor catalyst, and TiO_2 support [12]. The synthesis method and silicon and aluminum sources are key in determining the properties of ZSM-5 [13]. ZSM-5 zeolite is fabricated via different silanization processes using tetraethoxysilane (TEOS) or $\text{Na}_2\text{SiO}_3 \cdot 9\text{H}_2\text{O}$ as silicon sources and aluminum salts as aluminum sources. Among other silicon and aluminum sources, natural clay is considered an alternative source for zeolite synthesis owing to its low cost and abundance. Highly crystalline ZSM-5 has been prepared using natural clay [14].

In this study, the authors synthesized ZSM-5 via a hydrothermal method using domestic kaolin clay and sodium silicates as aluminum and silicon sources, respectively. The as-synthesized ZSM-5 was used to prepare $\text{TiO}_2/\text{ZSM-5}$ catalysts, which were characterized using modern analysis techniques. Furthermore, the photocatalytic performance of $\text{TiO}_2/\text{ZSM-5}$ composites was evaluated by the degradation of RhB under UV irradiation. The degradation kinetics and possible mechanism were investigated.

2. MATERIALS AND METHODS

Chemicals. Kaolin clay was obtained from Longyan city in China. Sodium hydroxide (NaOH), sodium silicate, absolute ethyl alcohol (EtOH), tetrapropyl ammonium bromide (TPABr), hydrogen peroxide (30%, H₂O₂), and tetrabutyltitanate (TBOT) were purchased from Sinopharm Chemical Reagent Co., Ltd. The Rhodamine B (RhB) was obtained from Sigma-Aldrich. All chemical agents were used without any purification.

Synthesis of ZSM-5 and TiO₂/ZSM-5 catalyst. SM-5 was synthesized via a hydrothermal method using kaolin clay and sodium silicate as aluminum and silicon sources [14]. First, 6.0 g of kaolin clay and 10.0 g of sodium silicate were dissolved in 100 cm³ of distilled water. Then, 1.6 g of NaOH and 3.0 g of TPABr were added, and the mixture was stirred at 150 rpm at room temperature for 24 h using a magnetic stirrer to form a homogeneous solution. Next, the homogeneous solution was carefully poured into a high-pressure reactor and heated in an oven (DHG-9036A, Shanghai Jinghong, China) at 180 °C for 24 h, and precipitate (the original ZSM-5) was obtained. The original ZSM-5 was washed three times with distilled water and dried at 80 °C for 8 h in a drying oven. Finally, the original ZSM-5 was calcined in an oven (KSL-1200X, HF-Kejing, China) from room temperature to 550 °C at a heating rate of 5 °C/min, and then held for 6 h to form ZSM-5. Further, a sol-gel method was employed to prepare the TiO₂/ZSM-5 composite catalyst denoted as TiO₂/ZSM-5(*X*) (the mass ratio of ZSM-5 to TiO₂). For example, TiO₂/ZSM-5(5) indicated that 6.0 g of ZSM-5 was added to the solution containing 3 cm³ of H₂O, 25 cm³ of EtOH, 2 cm³ of H₂O₂ as the stabilizing agent, and 5.13 cm³ of TBOT with 8 h continuous stirring. Then, the solution was filtered using a centrifugal filter (H-2050R, Changsha-Xiangyi, China), washed with EtOH, and dried at 80 °C for 12 h in a drying oven (DHG-9031A, Jinghong, China) and calcined from room temperature to 550 °C at a heating rate of 5 °C/min and then held for 2 h. TiO₂/ZSM-5(3) and TiO₂/ZSM-5(1) were also prepared following the same procedure. Pure TiO₂ was prepared by a similar method but without adding ZSM-5. Figure 1 shows a schematic of the synthesis procedure for TiO₂/ZSM-5 catalysts.

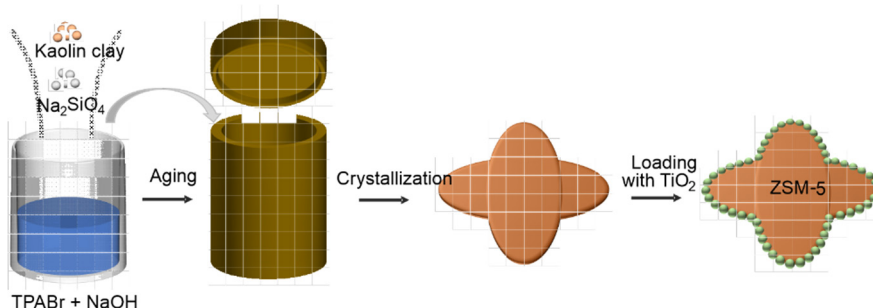


Fig. 1. Synthesis procedure of TiO₂/ZSM-5 catalysts

Characterization of ZSM-5 and TiO₂/ZSM-5 catalysts. The synthesized samples were characterized by powder X-ray diffraction (XRD) (X'pert MPD Pro, Philips, Holland), N₂ adsorption-desorption isotherms (TriStar 3020, Micromeritics, USA), UV-Vis diffuse reflectance spectra (UV-101, Hitachi, Japan), and scanning electron microscopy (SEM) (SU-70, Hitachi, Japan). The chemical composition of kaolin clay was analyzed by X-ray fluorescence spectroscopy (XRF) (SRS3400, Bruker). XRD patterns were obtained using a Rigaku D/max-rB diffractometer with graphite monochromatized Cu-K α radiation generated at 40 kV, 40 mA, and scanning 2θ of 5–60°. The special surface area, pore volume, and pore diameter of the samples were obtained from the N₂ adsorption-desorption isotherm operated at 77 K. The micropore-size distribution of all as-synthesized samples was analyzed by the Horvath–Kawazoe (HK) method. The optical properties were determined by UV-Vis spectrometry. All as-synthesized samples were directly observed under SEM operated at an acceleration voltage of 5 kV. The microstructures of the as-synthesized samples were determined using an optical microscope (MF600D-TFBD, Canon, Japan), and the submicroscopic structures were observed using a transmission electron microscope (TEM, Tecnai F30, FEI, American) with an accelerating voltage of 300 kV.

Photocatalytic performance evaluation. A quartz photoreactor was kept in a steel container with a magnetic stirrer. A 40 W high-pressure mercury lamp was used as a light source. The lamp was placed 10 cm above the RhB solution. The initial RhB dye solution was 5.0 mg/dm³. The RhB dye was degraded by a 1.0 g/dm³ TiO₂/ZSM-5 catalyst under UV light. For the degradation experiment, RhB dye was dissolved in distilled water, the solution pH was close to 7, and the experiment was conducted at room temperature. Each experiment was repeated three times, and the average values were recorded. After 30 min stirring in a dark condition as a background reaction, the concentration of RhB decreased, which is attributed to the adsorption by the catalyst. In the beginning, the UV lamp was turned on and irradiated for 60 min. The catalytic activity of all samples was evaluated by the degradation of the RhB solution under UV light. Then, the absorbance of the supernatant was recorded at a maximum absorption wavelength of 450–600 nm using a UV-Vis spectrophotometer (UV-2550, Shimadzu, Japan) and transformed into the concentration of RhB based on the calibration of a standard curve. To further demonstrate the photostability performance of the composite catalyst, TiO₂/ZSM-5(5) was repeatedly used four times to degrade the RhB dye solution (5 mg/dm³).

3. RESULTS AND DISCUSSION

The XRF results of kaolin clay are listed in Table 1. The sample contained 90.32% and 9.68% of Al₂O₃ and SiO₂, respectively, indicating that Al₂O₃ and SiO₂ are dominant in kaolin clay, and the molar ratio of SiO₂ to Al₂O₃ is close to 1.6 [15].

Table 1

The components of kaolin clay

Component	Percentage [wt. %]	Phase	Percentage [wt. %]
Al ₂ O ₃	34.92	kaolinite	90.32
SiO ₂	55.40	others	9.68
CaO	3.91		
V ₂ O ₅	0.10		
MnO	0.07	total	100
Fe ₂ O ₃	0.32		
Rb ₂ O	0.07		
ZrO ₂	0.01		
Nb ₂ O ₅	0.02		

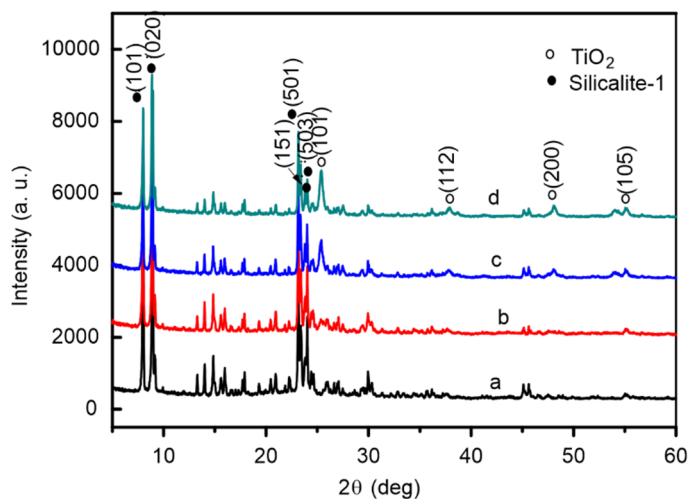


Fig. 2. XRD patterns of a) ZSM-5, b) TiO₂/ZSM-5, c) TiO₂/ZSM-5(3), and d) TiO₂/ZSM-5(1)

ZSM-5 prepared by mixing kaolin clay and sodium silicate was used as a support for TiO₂/ZSM-5 catalysts. Figure 2 shows the XRD patterns of the synthesized ZSM-5 and TiO₂/ZSM-5 catalysts containing different amounts of TiO₂. All samples displayed five definite peaks at 7.98°, 8.82°, 23.18°, 24.02°, and 24.46°, which are ascribed to the (101), (020), (503), (151), and (303) reflections, respectively, indicating that all as-synthesized samples exhibit the MFI-type structure [16]. The loading of TiO₂ could not break the MFI-type structure. Curves b–d show the XRD patterns of TiO₂/ZSM-5(5), TiO₂/ZSM-5(3), and TiO₂/ZSM-5(1), respectively. Four common diffraction peaks observed at 25.23°, 37.82°, 48.05°, and 53.91°, attributed to the (101), (112), (200), and (105) planes, were affected by the reflection of the anatase of TiO₂ [17]. Comparing TiO₂/ZSM-5(5) and TiO₂/ZSM-5(1), we find that the intensities of the 25.23°, 37.82°,

48.05°, and 53.91° peaks increased with an increase in the amount of TiO₂, confirming that ZSM-5 was loaded with TiO₂.

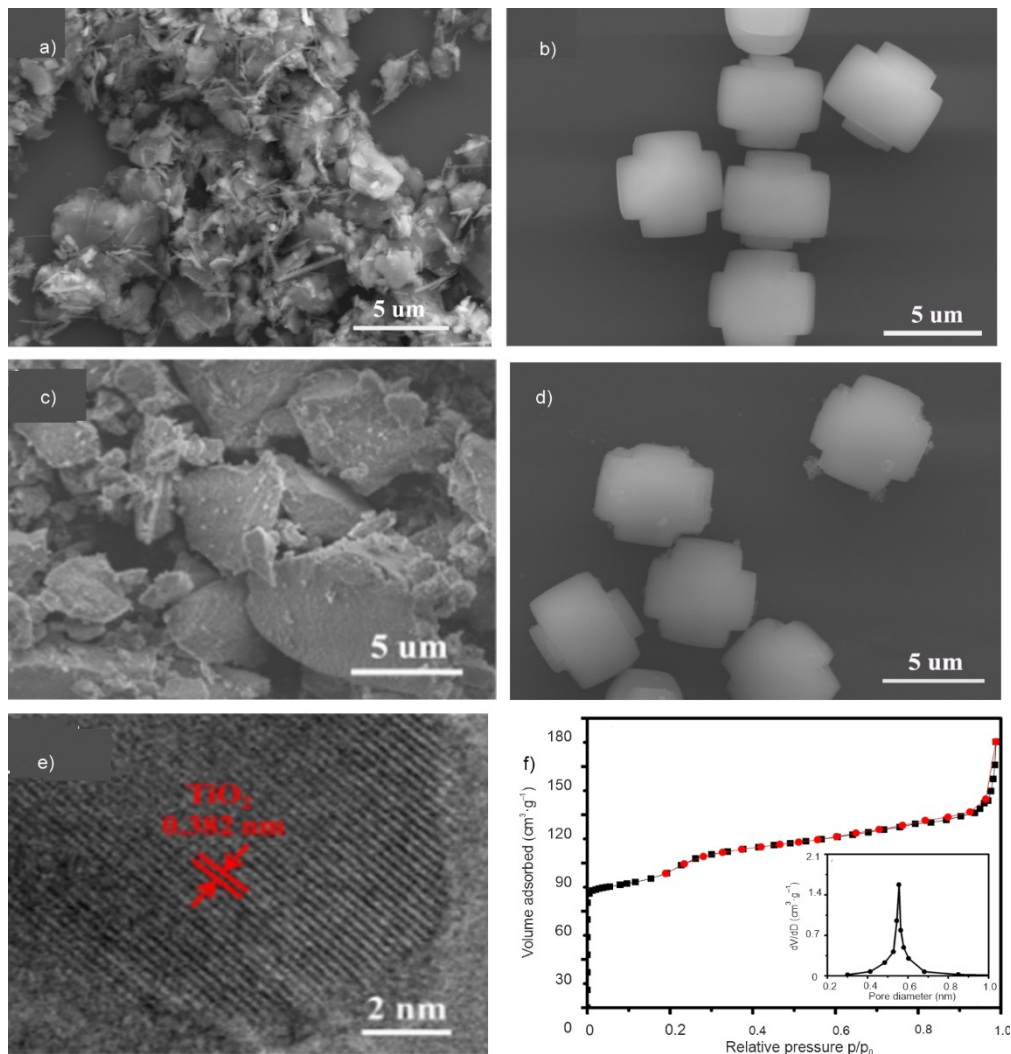


Fig. 3. SEM images of kaolin clay (a), ZSM-5 (b), TiO₂ (c), TiO₂/ZSM-5 (d), TEM image of TiO₂/ZSM-5 (e), N₂ adsorption-desorption isotherms, and pore size distribution of TiO₂/ZSM-5 (f)

Figures 3a–3d show SEM images of kaolin clay, ZSM-5, TiO₂, and TiO₂/ZSM-5. Figures 3e and 3f show the TEM image and pore-size distribution of TiO₂/ZSM-5, respectively. Figure 3a shows the schistose and acicular shapes of the kaolin clay. ZSM-5 showed uniform small particles with a size of 5 μm, and a twinned hexagonal crystal shape without extra particles. Pure TiO₂ was well bonded together, as shown in Fig. 3c. SEM

image of TiO₂/ZSM-5(5) revealed a ZSM-5:TiO₂ ratio of 5:1. TiO₂ nanoparticles were evenly dispersed in a solution before deposition onto ZSM-5. Furthermore, TiO₂ content in TiO₂/ZSM-5 was less than that of ZSM-5. Consequently, only small amounts of TiO₂ nanoparticles were loaded on the surface of ZSM-5, which is consistent with the result reported by Huang et al. [18]. The TEM image of the TiO₂/ZSM-5 catalyst shows the lattice fringes of 0.382 nm spacing corresponding to TiO₂.

The N₂ adsorption-desorption isotherms and micropore size distribution of TiO₂/ZSM-5, (Fig. 3f) were analyzed using the HK method. They reveal a significantly high uptake in the region with P/P₀ less than 0.1, indicating microporosity in ZSM-5 [17]. The BET data of ZSM-5 show that it has a surface area of 364 m²/g. ZSM-5 showed a narrow micropore size distribution of 0.5–0.55 nm. The high BET surface area of ZSM-5 increases the dispersion of TiO₂ and enhances the adsorption of reactants on the catalyst surface, improving the photocatalytic efficiency [19].

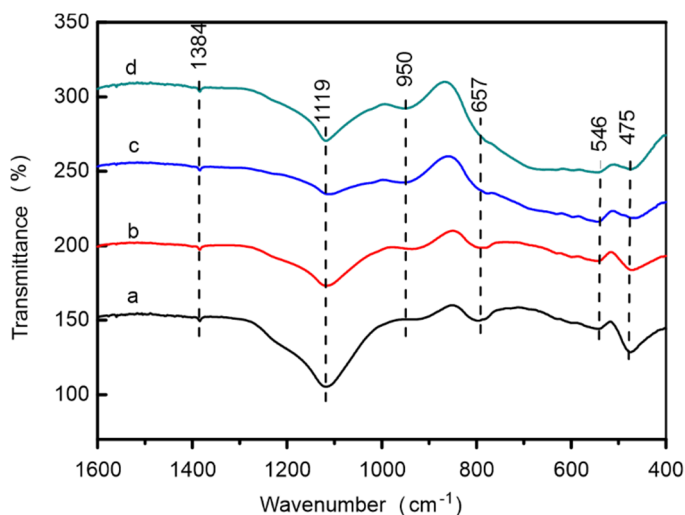


Fig. 4. FT-IR spectra of ZSM-5 (a), TiO₂/ZSM-5(5) (b), TiO₂/ZSM-5(3) (c), TiO₂/ZSM-5(1) (d)

The FT-IR spectra of ZSM-5 and composite TiO₂/ZSM-5 catalysts containing different amounts of TiO₂ are shown in Fig. 4. All samples showed consistent vibration bands at 475, 546, 795, 950, and 1119 cm⁻¹. The bands at 1119 and 795 cm⁻¹ are attributed to the internal asymmetric stretching vibration and external symmetric stretching of Si–O–Si bonds of ZSM-5, respectively [20]. The band at 950 cm⁻¹ was assigned to the stretching vibration of the Si–OH group [21], and that at 546 cm⁻¹ is attributed to five-membered rings of the Ti–Si pentasil zeolite structure [22]. Finally, the band at 475 cm⁻¹ was assigned to the bending vibration of SiO₄. We infer that the structure of ZSM-5 is complete when ZSM-5 is loaded with TiO₂ based on the conformable XRD patterns of

ZSM-5 and composite TiO₂/ZSM-5. FT-IR spectra of TiO₂/ZSM-5(5), TiO₂/ZSM-5(1), and TiO₂/ZSM-5(3) correspond to curves b–d in Fig. 4. The series of TiO₂/ZSM-5 catalysts showed a wide band from 504 to 657 cm⁻¹, which corresponds to the Ti–O–Ti vibration. The absorption peak corresponding to TiO₂ became more obvious with an increased TiO₂ content, which is consistent with the XRD result.

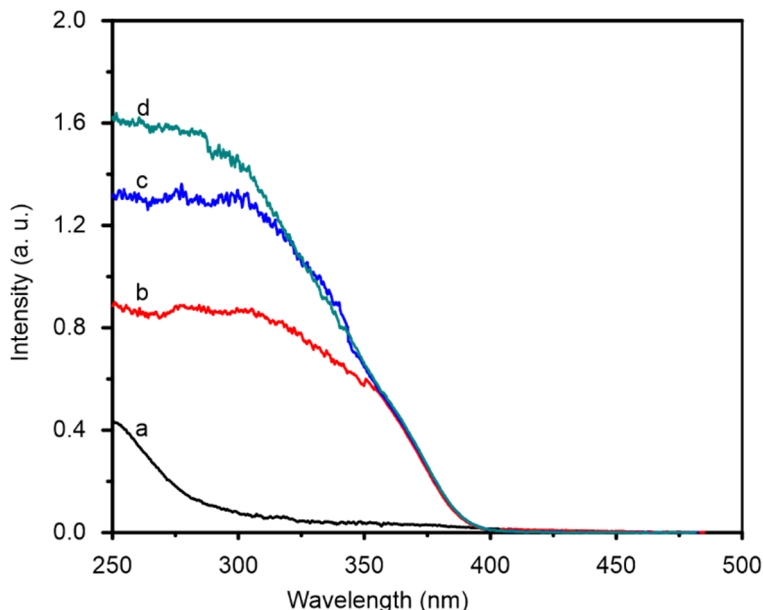


Fig. 5. UV-Vis spectra of ZSM-5 (a), TiO₂/ZSM-5(5) (b), TiO₂/ZSM-5(3) (c), TiO₂/ZSM-5(1) (d)

Figure 5 shows UV-Vis diffuse reflectance spectra of ZSM-5 and composite TiO₂/ZSM-5 catalysts containing different amounts of TiO₂. ZSM-5 showed a weak absorption band at about 250–280 nm (Fig. 5a). A broad absorption band was observed at 380 nm (Fig. 5b) when ZSM-5 was loaded with 20% of TiO₂. With an increase in TiO₂ content, the intensity of the absorption band of TiO₂/ZSM-5 catalysts continuously increased. Interestingly, the broad absorption bands of the catalysts were similar between 380 and 400 nm, indicating that the TiO₂/ZSM-5 catalysts with different amounts of TiO₂ have similar bandgap (ca. 3.2 eV) [23].

The textural properties of ZSM-5 and TiO₂/ZSM-5 catalysts containing different amounts of TiO₂ are listed in Table 2. The BET and t-plot revealed a surface area of 364 m²/g for ZSM-5, and that of TiO₂/ZSM-5(5), TiO₂/ZSM-5(3), and TiO₂/ZSM-5(1) are 315, 303, 289 m²/g, respectively, indicating a decrease in BET surface area with an increase in the ZSM-5/TiO₂ ratio. The increase in the BET surface area of the photocatalyst increases the available adsorption sites, and consequently, prevents the recom-

bination of photogenerated electron–hole pairs, thereby increasing the rate of photocatalysis [24]. The photocatalytic performance of the TiO₂/ZSM-5 catalysts was evaluated by the decomposition of organic RhB dye.

Table 2

Textural properties of ZSM-5 and TiO₂/ZSM-5 with different amounts of TiO₂

Sample	S_{BET} [m ² /g]	S_{ext} [m ² /g]	V_{total} [cm ³ /g]	D_{HK} [nm]
ZSM-5	364	182.4	0.07	0.54
TiO ₂ /ZSM-5(5)	315	171.6	0.08	0.54
TiO ₂ /ZSM-5(3)	303	166.9	0.08	0.54
TiO ₂ /ZSM-5(1)	289	152.8	0.07	0.53
Pure TiO ₂	19.5	11.5	0.07	0.42

S_{BET} – the specific area determined by the Brunauer–Emmet–Teller method, S_{ext} – internal specific surface area, V_{total} – the total pore volume, and D_{HK} – pore diameter determined by the Horvath–Kawazoe method.

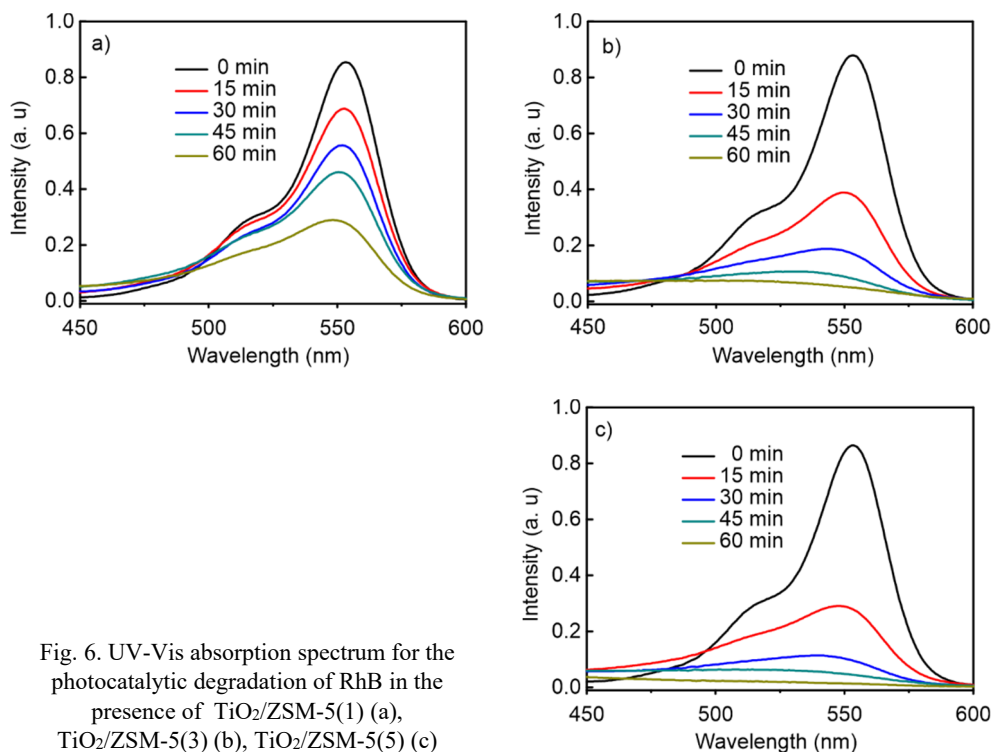


Fig. 6. UV-Vis absorption spectrum for the photocatalytic degradation of RhB in the presence of TiO₂/ZSM-5(1) (a), TiO₂/ZSM-5(3) (b), TiO₂/ZSM-5(5) (c)

The photocatalytic activity of $\text{TiO}_2/\text{ZSM-5}$ catalysts for the decomposition of RhB in an aqueous solution under UV irradiation was tested. Figure 6 shows the UV-Vis absorption spectrum for the photocatalytic degradation of RhB in the presence of $\text{TiO}_2/\text{ZSM-5}(5)$, $\text{TiO}_2/\text{ZSM-5}(3)$, and $\text{TiO}_2/\text{ZSM-5}(1)$ under UV light with wavelengths ranging from 250 to 270 nm. First, all RhB solutions were dispersed in the dark using a magnetic stirrer to achieve adsorption–desorption equilibrium, after which they were irradiated by UV light. After 1-h irradiation, the RhB solution still showed a strong UV-Vis absorbance spectrum of RhB (Fig. 6a). With an increase in TiO_2 content, the UV-Vis absorbance spectrum of the catalyst gradually became weaker (Figs. 6b and 6c, and $\text{TiO}_2/\text{ZSM-5}(5)$ catalyst showed the highest photocatalytic activity.

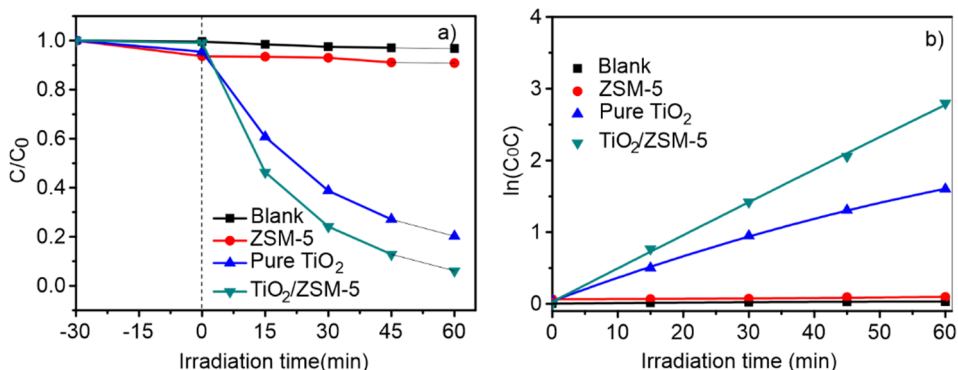


Fig. 7. Photocatalytic degradation (a) and kinetics (b) of blank, ZSM-5, $\text{TiO}_2/\text{ZSM-5}(5)$, and pure TiO_2 for degradation of RhB in the dark and under UV light irradiation

Figure 7a shows that only 2.8% of RhB underwent self-degradation, even after 60-min irradiation. However, under the dark condition, the photocatalytic dye decomposition curve of ZSM-5 was 6.0%, which is slightly higher than that of $\text{TiO}_2/\text{ZSM-5}$ (4.1%) because there was only catalytic adsorption. This is consistent with the BET results, which show that the BET surface area of ZSM-5 is larger than that of $\text{TiO}_2/\text{ZSM-5}$. Only ZSM-5 could not further remove RhB under continuous UV irradiation, confirming that ZSM-5 is not photoactive for RhB decomposition. However, $\text{TiO}_2/\text{ZSM-5}$ could significantly remove the dye, indicating that TiO_2 exhibits excellent photoactivity, which is consistent with the results of Suwarnka et al. [25]. $\text{TiO}_2/\text{ZSM-5}(5)$ showed a maximum photodegradation of 98.53%, which is higher than the 80.13% shown by pure TiO_2 . The RhB removal is attributed to the synergistic effect of ZSM-5 and TiO_2 . The kinetics of all as-synthesized samples for RhB degradation under UV light irradiation is shown in Fig. 7b. The photocatalytic degradation can be described by pseudo-first-rate-order kinetics, $\ln(C_0/C) = kt$, where k is a pseudo-first-rate kinetic constant, t is the irradiation time (min), C_0 and C denote the RhB initial and final concentration (mg/dm^3). The calculated k value for $\text{TiO}_2/\text{ZSM-5}(5)$ is 0.063, which is 2.1 times that

of pure TiO₂. Thus, the photocatalytic activity of the TiO₂/ZSM-5 catalyst is significantly higher than that of TiO₂.

Photocatalytic reactions by TiO₂ under UV irradiation have higher energy than the TiO₂ bandgap. Figure 8 shows a schematic of the adsorption and photocatalytic degradation mechanism of RhB molecules on TiO₂/ZSM-5 catalyst. The conduction electron band (e⁻) and valence hole band (h⁺) were generated when an aqueous TiO₂/ZSM-5 suspension was irradiated by UV light, forming reactive oxygen species. Holes, [•]OH radical, and [•]O₂ can effectively oxidize, degrade, and mineralize RhB molecules [26]. The adsorption of RhB molecules on the TiO₂/ZSM-5 catalysts is attributed to the high surface area of ZSM-5, resulting in the formation of a high concentration of RhB on the ZSM-5 surface. When TiO₂/ZSM-5 catalyst is irradiated by UV light, TiO₂ can generate strong oxidation potential to degrade RhB owing to the formation of hydroxyl radicals and valence band holes [27], implying that a composite catalyst for field applications can be obtained by combining TiO₂ and ZSM-5.

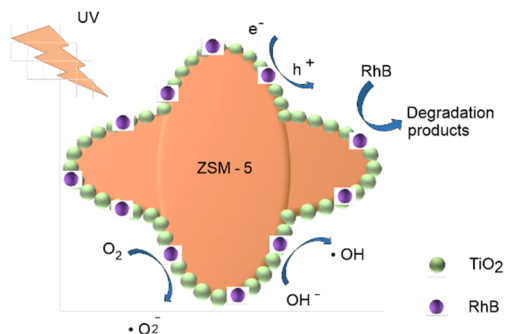


Fig. 8. Schematic diagram for the adsorption and photocatalytic degradation of RhB molecules on a catalyst

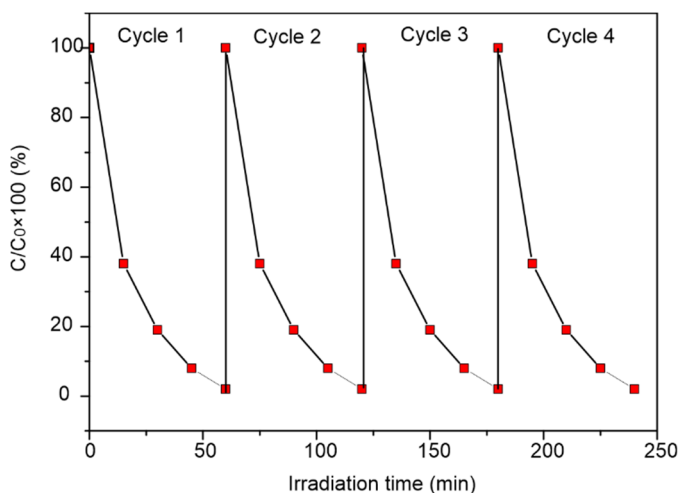


Fig. 9. Four photocatalytic degradation cycles of RhB using TiO₂/ZSM-5(5) under UV light ($M_{\text{catalyst}} = 1 \text{ g/dm}^3$, $C_{0(\text{RhB})} = 5 \text{ mg/dm}^3$)

To investigate the photostability of the composite catalysts, 5 mg/dm³ of RhB dye was degraded four times using 1 g/dm³ of TiO₂/ZSM-5(5) (Fig. 9). TiO₂/ZSM-5(5) showed high photostability after four photocatalytic degradation cycles. The photocatalytic efficiency decreased by only 2.5%, indicating that TiO₂ nanoparticles adhered tightly to the ZSM-5 surface.

4. CONCLUSION

Composite TiO₂/ZSM-5 catalysts were synthesized and evaluated for photocatalytic degradation of RhB dyes under UV irradiation. The catalysts showed high surface area, strong UV absorption, and a small bandgap. The high BET surface area of ZSM-5 increases the dispersion of TiO₂, increasing the number of available adsorption sites, which prevents the recombination of photogenerated electron–hole pairs. Thus, the rate of photocatalysis is increased. Under optimum conditions, TiO₂/ZSM-5 showed 98.53% RhB removal under UV irradiation, which is higher than that of pure TiO₂ (80.13%), indicating that the combination of adsorption and photocatalytic degradation enhanced the RhB removal. After four photocatalytic degradation cycles, only a 2.5% reduction in the removal efficiency of the catalysts was observed, confirming that TiO₂ nanoparticles adhered tightly to the ZSM-5 surface. This study serves as a good basis for investigating TiO₂/ZSM-5 catalysts to promote their applications in reducing the environmental pollution.

ACKNOWLEDGEMENTS

The authors express their gratitude to the National Science Foundation for Young Scholars of China (Grant No. 51406141), the National Science Foundation for Fujian Province, China (Grant No. 2019J01830), the New-Century Training Program Foundation for Fujian Province, China (Grant No. 2017), the Scientific Research Project of Wuyi University (YJ201703) for providing the support of the budget. The authors also appreciate the help from the staff working at Wuyi University and Tajen University, especially for the students involved in this experiment.

REFERENCES

- [1] MIYAKE K., YAMADA M., SUGIURA Y., HIROTA Y., UCHIDA Y., NISHIYAMA N., *Synthesis of mesoporous MFI zeolite by dry gel conversion with ZnO particles and the catalytic activity on TMB cracking*, J. Porous Mat., 2016, 23, 311–316. DOI: 10.1007/s10934-015-0083-x.
- [2] HU J., LI H., MUHAMMAD S., WU Q., ZHAO Y., JIAO Q., *Surfactant-assisted hydrothermal synthesis of TiO₂/reduced graphene oxide nanocomposites and their photocatalytic performances*, J. Solid State Chem., 2017, 253, 113–120. DOI:10.1016/j.jssc.2017.05.034.
- [3] YANG X., CUI H., LI Y., QIN J., ZHANG R., TANG H., *Fabrication of Ag₃PO₄-graphene composites with highly efficient and stable visible light photocatalytic performance*, ACS Catal., 2013, 3, 363–369. DOI: 10.1021/cs3008126.

- [4] XU X., YANG G., LIANG J., DING S., TANG C., YANG H., YAN W., YANG G., YU D., *Fabrication of one-dimensional heterostructured TiO₂@SnO₂ with enhanced photocatalytic activity*, J. Mater. Chem. A, 2014, 2, 116–122. DOI: 10.1039/c3ta12863f.
- [5] ZHANG L.J., LI S., LIU B.K., WANG D.J., XIE T.F., *Highly efficient CdS/WO₃ photocatalysts: z-scheme photocatalytic mechanism for their enhanced photocatalytic H₂ evolution under visible light*, ACS Catal., 2014, 4, 3724–3729. DOI: 10.1021/cs500794j.
- [6] XIE T., LIU C., XU L., YANG J., ZHOU W., *Novel heterojunction Bi₂O₃/SrFe₁₂O₁₉ magnetic photocatalyst with highly enhanced photocatalytic activity*, J. Phys. Chem. C, 2013, 117, 24601–24610. DOI: 10.1021/jp408627e.
- [7] TIMOUMI S.N., ALAMRI H., *The development of TiO₂-graphene oxide nano composite thin films for solar cells*, Res. Phys., 2018, 11, 46–51. DOI: 10.1016/j.rinp.2018.06.017.
- [8] DONG C., XING M., ZHANG J., *Economic hydrophobicity triggering of CO₂ photoreduction for selective CH₄ generation on noble-metal-free TiO₂-SiO₂*, J. Phys. Chem. Lett., 2016, 7, 2962–2966. DOI: 10.1021/acs.jpcclett.6b01287.
- [9] SUWARNKAR M.B., DHALABBE R.S., KADAM A.N., GARADKAR K.M., *Enhanced photocatalytic activity of Ag doped TiO₂ nanoparticles synthesized by a microwave assisted method*, Ceram. Int., 2014, 40, 5489–5496. DOI: 10.1016/j.ceramint.2013.10.137.
- [10] ANDERSON C., BARD A.J., *Improved photocatalytic activity and characterization of mixed TiO₂/SiO₂ and TiO₂/Al₂O₃ materials*, J. Phys. Chem. B, 1997, 101, 2611–2616. DOI: 10.1021/jp9626982.
- [11] TAKEUCHI M., DEGUCHI J., HIDAKA M., SAKAI S., WOO K., CHOI P.P., PARK J.K., ANPO M., *Enhancement of the photocatalytic reactivity of TiO₂ nano-particles by a simple mechanical blending with hydrophobic mordenite (MOR) zeolite*, Appl. Catal. B: Environ., 2009, 89, 406–410. DOI: 10.1016/j.apcatb.2008.12.022.
- [12] ZNAD H., ABBAS K., HENA S., AWUAL M.R., *Synthesis a novel multilamellar mesoporous TiO₂/ZSM-5 for photo-catalytic degradation of methyl orange dye in aqueous media*, J. Environ. Chem. Eng., 2018, 6, 218–227. DOI: 10.1016/j.jece.2017.11.077.
- [13] CHEN X.S., JIANG R.L., ZHOU Z.H., WANG X.W., *Synthesis and catalytic properties of ZSM-5 crystals with different morphologies in gelatin hydrogels*, J. Disp. Sci. Technol., 2019, 1–8, 561–568. DOI: 10.1080/01932691.2019.1703735.
- [14] SHEN K., QIAN W., WANG N., ZHANG J., WEI F., *Direct synthesis of c-axis oriented ZSM-5 nanoneedles from acid-treated kaolin clay*, J. Mater. Chem. A, 2013, 1, 3272–3275. DOI: 10.1039/c3ta01479g.
- [15] MIGNONI M.L., PETKOWICZ D.I., FERNANDES M.N., PERGHER S.B., *Synthesis of mordenite using kaolin as Si and Al source*, Appl. Clay Sci., 2008, 41, 99–104. DOI: 10.1016/j.clay.2007.09.010.
- [16] YEONG Y.F., ABDULLAH A.Z., AHMAD A.L., BHATIA S., *Process optimization studies of p-xylene separation from binary xylene mixture over silicalite-1 membrane using response surface methodology*, J. Memb. Sci., 2009, 341, 96–108. DOI: 10.1016/j.memsci.2009.05.042.
- [17] MENG Z., ZHANG X., QIN J., *A high efficiency microfluidic-based photocatalytic microreactor using electrospun nanofibrous TiO₂ as a photocatalyst*, Nanosc., 2013, 5, 4687–4690. DOI: 10.1039/c3nr00775h.
- [18] HUANG H.B., HUANG H.L., FENG Q.Y., LIU G.Y., ZHAN Y.J., WU M.Y., LU H.X., SHU Y.J., LEUNG D.Y.C., *Catalytic oxidation of benzene over Mn modified TiO₂/ZSM-5 under vacuum UV irradiation*, Appl. Catal., B: Environ., 2017, 203, 870–878. DOI: 10.1016/j.apcatb.2016.10.083.
- [19] ELROZ M., LAKISS L., ELFALLAH J., LEBEDEV O.I., THIBAUT S.F., VALTCHEV V., *Incorporation of clusters of titanium oxide in beta zeolite structure by a new cold TiCl₄-plasma process: physicochemical properties and photocatalytic activity*, Phys. Chem. Chem. Phys., 2013, 15, 16198–16207. DOI: 10.1039/c3cp52478g.
- [20] QIAN X., DU J., LI B., SI M., YANG Y., HU Y., NIU G., ZHANG Y., XU H., TU B., TANG Y., ZHAO D., *Controllable fabrication of uniform core-shell structured zeolite@SBA-15 composites*, Chem. Sci., 2011, 2, 2006–2016. DOI: 10.1039/c1sc00250c.

- [21] BLASCO T., CORMA A., NAVARRO M.T., PARIENTE J.P., *Synthesis, characterization, and catalytic activity of Ti-MCM-41 structures*, J. Catal., 1995, 156, 65–74. DOI: 10.1006/jcat.1995.1232.
- [22] MEHDIPOURGHASI M., MOHEB A., KAZEMIAN H., *Incorporation of boron into nano-size MFI zeolite structure using a novel microwave-assisted two-stage varying temperatures hydrothermal synthesis*, Micropor. Mesopor. Mat., 2010, 136, 18–24. DOI: 10.1016/j.micromeso.2010.07.011.
- [23] WANG L., ZHANG J., WANG A., *Fast removal of methylene blue from aqueous solution by adsorption onto chitosan-g-poly (acrylic acid)/attapulgitite composite*, Desalin., 2011, 266, 33–39. DOI: 10.1016/j.desal.2010.07.065.
- [24] MOHAMED R.M., ISMAIL A.A., OTHMAN I., IBRHIM I.A., *Preparation of TiO₂-ZSM-5 zeolite for photodegradation of EDTA*, J. Mol. Catal. A: Chem., 2005, 238, 151–157. DOI: 10.1016/j.molcata.2005.05.023.
- [25] SUWARANKAR M.B., KADAM A.N., KHADE G.V., GAVADEL N.L., GARADKAR K.M., *Modification of TiO₂ nanoparticles by HZSM-5 for the enhancement in photodegradation of Acid Green 25*, J. Mater. Sci.: Mater. Electron., 2016, 27, 843–851. DOI: 10.1007/s10854-015-3825-2.
- [26] LI R., JIA Y., WU J., ZHEN Q., *Photocatalytic degradation and pathway of oxytetracycline in aqueous solution by Fe₂O₃-TiO₂ nanopowder*, RSC Adv., 2015, 5, 40764–40771. DOI: 10.1039/c5ra04540a.
- [27] GRABOWSKA E., RESZCZYNSKA J., ZALESKA A.R., *Mechanism of phenol photodegradation in the presence of pure and modified-TiO₂: A review*, Water Res., 2013, 46, 5453–5471. DOI: 10.1016/j.watres.2012.07.048.